Received: 26 May 2017 | Revised: 12 September 2017 | Accepted: 14 September 2017

DOI: 10.1002/er.3918

RESEARCH ARTICLE

WILEY INTERNATIONAL JOURNAL OF ENERGY RESEARCH

# Carbon supported bimetallic Ru-Co catalysts for $H_2$ production through $NaBH_4$ and $NH_3BH_3$ hydrolysis

R. Fiorenza[1] | S. Scirè[1] | A.M. Venezia[2]

[1]Dipartimento di Scienze Chimiche, Università di Catania, Viale A. Doria 6, Catania 95125, Italy

[2]Istituto per lo Studio dei Materiali Nanostrutturati CNR, Via Ugo La Malfa 153, Palermo 90146, Italy

**Correspondence**
S. Scirè, Dipartimento di Scienze Chimiche, Università di Catania, Viale A. Doria 6, Catania 95125, Italy.
Email: sscire@unict.it; salvatorescire.ct@gmail.com

**Summary**

This work investigates the effect of the addition of small amounts of Ru (0.5-1 wt%) to carbon supported Co (10 wt%) catalysts towards both $NaBH_4$ and $NH_3BH_3$ hydrolysis for $H_2$ production. In the sodium borohydride hydrolysis, the activity of Ru-Co/carbon catalysts was sensibly higher than the sum of the activities of corresponding monometallic samples, whereas for the ammonia borane hydrolysis, the positive effect of Ru-Co systems with regard to catalytic activity was less evident. The performances of Ru-Co bimetallic catalysts correlated with the occurrence of an interaction between Ru and Co species resulting in the formation of smaller ruthenium and cobalt oxide particles with a more homogeneous dispersion on the carbon support. It was proposed that $Ru^{\circ}$, formed during the reduction step of the Ru-Co catalysts, favors the $H_2$ activation, thus enhancing the reduction degree of the cobalt precursor and the number of Co nucleation centers. A subsequent reduction of cobalt and ruthenium species also occurs in the hydride reaction medium, and therefore the state of the catalyst before the catalytic experiment determines the state of the active phase formed in situ. The different relative reactivity of the Ru and Co active species towards the two investigated reactions accounted for the different behavior towards $NaBH_4$ and $NH_3BH_3$ hydrolysis.

**KEYWORDS**

activated carbon, ammonia borane, cobalt, fuel cells, ruthenium, sodium borohydride

## 1 | INTRODUCTION

The use of hydrogen as energy transporter appears as a key factor to boost the transition from fossil fuels to renewable energy in the frame of a sustainable future.[1,2] Hydrogen has the key advantage of being a clean and energetic fuel but also needs tricky steps to be produced, purified, stored, and distributed. In particular, the storage of $H_2$ represents both a scientific and technical challenge.

Among $H_2$ storage materials, as carbon nanostructures,[3] metal-organic frameworks,[4] alcohols,[5] formic acid,[6,7] chemical hydrides attracted special attention because of their high gravimetric/volumetric $H_2$ storage capacities,[8] being also a suitable pure $H_2$ source for PEM fuel cell technology,[9] mainly for portable applications, like computers and cellular phones.

Chemical hydrides are able to produce $H_2$ by means of a simple hydrolysis reaction and, generally, exhibit good stability during their storage before use. Among different hydrides, sodium borohydride ($NaBH_4$, thereinafter denoted SB) has been up to now regarded as the most promising, due to good $H_2$ storage capacity (10.9 wt%), high stability in alkaline solution, and nonflammability of this hydride.[10] The $NaBH_4$ hydrolysis for hydrogen production ($NaBH_4 + 2H_2O \leftrightarrow NaBO_2 + 4H_2$) is an exothermic reaction occurring even at 0°C, with the nontoxic

  

sodium metaborate ($NaBO_2$) as only by-product. At pH > 13, $NaBH_4$ is stable, $H_2$ release taking place only in the presence of suitable catalysts, such as Ru,[11,12] Co,[13,14] Pt,[15,16] Ni,[17] or Pd,[18] leading to "hydrogen on demand" systems.[9,10] A recent study of Demirci[9] pointed out as 98% of the papers dedicated to catalysis of SB hydrolysis were focused on heterogeneous supported metal catalysts, whereas only 2% used homogeneous catalysts. The use of heterogeneous catalysts allows an easy control of the $H_2$ generation rate just by acting on the flow of the hydride solution through the catalyst, making these systems more appropriate for hydrogen on demand applications.[9,10] A key parameter to take into account in the case of heterogeneous catalysts is the support used, which can significantly act on the performance of metal catalysts.[11] Most used supports in $NaBH_4$ hydrolysis were activated carbon,[9,11,19] alumina,[20] and ion exchange resins.[21]

More recently, ammonia borane ($NH_3BH_3$, coded AB) was accounted an interesting alternative to SB, exhibiting higher $H_2$ capacity (19.6 wt%) together with a low toxicity and a high stability in ambient conditions.[22,23] The stability of AB at pH 7 is of practical importance as it allows the use of a larger number of supports, as silica, ceria, and zeolites,[24-26] not suitable under the strongly basic pH conditions of the SB solution. Several catalysts have been found effective in accelerating $NH_3BH_3$ hydrolysis ($NH_3BH_3 + 2H_2O \rightarrow NH_4BO_2 + 3H_2$), namely, noble metals,[27,28] nonnoble metals,[29,30] and B-containing nanocomposites.[31]

For both SB and AB hydrolysis precious metal catalysts (Pt, Rh, and Ru) exhibited significantly better performance than nonnoble metal ones. Among noble metals, Ru catalysts are the favored alternative for both SB and AB hydrolysis as Ru is sensibly less expensive than Pt and Rh. In previous works, we found that Ru on activated carbons represents one of the best catalytic systems for the SB hydrolysis reaction, the Ru precursor and the support properties strongly affecting the catalytic performance.[11,19] The better performance of the carbon support compared to ceria, alumina, and titania was ascribed to both higher surface area and chemical inertness of the carbon at basic pH values required by SB hydrolysis.[11]

The scarcity of Ru or the high price of other noble metals encourage the exploration of new routes to reduce the amount of these metals or substitute them with less expensive ones with comparable catalytic properties. The most investigated element is cobalt, which well balances catalytic activity and cheapness.[1]

It is recognized that the performance of bimetallic catalysts is often superior as compared to the corresponding monometallics.[33,34] Up to now, the bimetallic alloy nanoparticles made of Co or Ni and noble metal (Rh, Ru) have emerged as catalysts with high performance for the hydrogen production by hydrolysis of both SB and AB.[35-37] For instance, Krishnan et al[35] reported that the efficiency of Pt-Ru bimetallic system towards SB hydrolysis is almost double of either Ru or Pt (all catalysts supported on $LiCoO_2$), whereas Rachiero et al[37] observed that Ru-Co alloys supported on $\gamma$-$Al_2O_3$ give higher $H_2$ generation rates in the AB hydrolysis than bare single monometallic samples. On this basis, we here investigated both the $NaBH_4$ and the $NH_3BH_3$ hydrolysis over mono and bimetallic Ru-Co/activated carbon catalysts with the aim to get a better insight on the mechanism of these reactions and on the role of ruthenium and cobalt species in affecting the catalytic performance of this system. As far as we know, this is the first paper comparing the hydrolysis of $NaBH_4$ and $NH_3BH_3$ over the same bimetallic catalytic system.

## 2 | EXPERIMENTAL

Mono and bimetallic Co and Ru supported catalysts were made by incipient wet (co)impregnation with water solutions of $Co(NO_3)_2$ (Sigma Aldrich) and $Ru(NO)(NO_3)_3$ (Alfa Aesar). The support was a vegetable activated carbon (Sicarb), obtained by exhausted olive cake with 1200 $m^2 \cdot g^{-1}$ surface area. The metal loading of catalysts was 10 wt% for Co and/or 0.5 to 1 wt% for Ru. Before use, catalysts were kept in an oven overnight at 120°C. Catalysts were coded Co/C for the monometallic Co sample and XRu/C and XRuCo/C for monometallic Ru and bimetallic Ru-Co samples, respectively, where X was the Ru wt%. It is worth to notice that in the presence of Ru and/or Co, the surface area of the carbon was not considerably modified according to both the relatively low metal loading and the high support porosity.

The experimental setup for the catalytic experiments consisted in a magnetically stirred batch glass reactor (100 mL) with 3 necks, the central one is used to allow entering the solution and the catalyst into the reactor, and the two other ones are used to measure the reaction temperature by a thermocouple and to convey and quantify the evolved $H_2$. To rule out temperature effects due to the exothermic reaction, the reaction temperature was kept constant (±0.3°C) using an externally circulating ethylene glycol and water mixture.

In the case of SB hydrolysis, $NaBH_4$ (Fluka, 96% purity) was dissolved in NaOH (4 wt% solution) to obtain 10 wt% sodium borohydride solution. Fifteen milliliters of this solution was added to 25 mL of NaOH (4 wt%) and transferred to the jacketed reactor. When the temperature

[1]References [8,9,13,14,17,20,26,29,32].

was stable, 0.1 g of the catalyst (14-20 mesh) was added in the reactor. The amount of produced $H_2$ was evaluated by a gas flowmeter.

In the case of AB hydrolysis, catalytic tests were performed using the water displacement method. Ten milligrams of catalyst (14-20 mesh particle size) was placed in the jacketed reaction flask thermostated at the chosen temperature (25°C, 35°C, or 45°C) with 10 mL of deionized water and kept under stirring. Twenty-five milligrams of AB powder were then added to the flask. The amount of the evolved $H_2$ was determined through an inverted, water-filled burette placed in a water-filled vessel.

Catalytic activity was reported as $H_2$ yield, namely, the fraction between the volume of produced $H_2$ and the stoichiometric one, and as initial rate, computed from the conversion curve slope against time ($t$) at $t = 0$.[11,19] Before each test, samples were reduced in situ in $H_2$ at 300°C for 1 hour.

Temperature programmed reduction ($H_2$-TPR) was measured under flow of 5 vol% $H_2$ in Ar using a TCD detector, heating the sample with a rate of 10°C/min. The effluent gas was analyzed by an online gas chromatograph, equipped with a packed column with 10% FFAP on Chromosorb W and a FID detector, and by a VG quadrupole mass spectrometer. Samples were dried before experiments in air at 120°C for 2 hours.

The BET method, with nitrogen adsorption at nitrogen liquid temperature, was used for determination of the surface area by means of a Sorptomatic 1990 instrument (Thermo Quest), outgassing samples at 120°C and $10^{-3}$ Torr before tests.

A Bruker instrument using Ni-filtered Cu $K_a$ radiation was used to perform X-ray diffraction (XRD) analysis. A proportional counter and a 2θ integration step size of 0.05° were used. The assignment of the crystalline phases was made using the JPDS powder diffraction file cards.[38] Before XRD measurements samples were treated ex situ in $H_2$ at 300°C for 1 hour.

X-ray photoelectron spectroscopy (XPS) analyses were performed with a VG Microtech ESCA 3000 Multilab, using the unmonochromatized AlKa source (1486.6 eV), operated at 14 kV and 15 mA. Pass energies of 50 and 20 eV were used, respectively, for the survey and the individual peak energy regions. Binding energies (precision of ±0.15 eV) of the powder samples were referenced to the C 1s binding energy of the carbon carrier, set at 284.5 eV. Qualitative and quantitative analysis of the peaks was performed with a software provided by VG performing the fitting procedure according to Shirley and Sherwood.[39,40] Before XPS measurements, samples were treated ex situ in $H_2$ at 300°C for 1 hour.

Transmission electron microscopy (TEM) photos were obtained on powdered samples by a Jeol, JEM 2010 instrument. After ultrasonication in ethanol, a few droplets of the sample suspension were deposited on a Cu grid coated by a holey carbon film and after evaporation of the solvent introduced into the microscope column. Before tests, samples were pretreated ex situ in $H_2$ at 300°C for 1 hour.

Metal dispersion was determined by CO pulse chemisorption at room temperature. Before measurements, samples were pretreated in situ in $H_2$ at 300°C for 1 hour.

## 3 | RESULTS AND DISCUSSION

### 3.1 | Catalytic activity and kinetic measurements

In Figure 1, the $H_2$ yields at 35°C in the $NaBH_4$ hydrolysis against reaction time over carbon supported mono and bimetallic Ru and Co catalysts are compared. In particular, Figure 1A shows the activity of the Ru-Co series with lower (0.5 wt%) Ru content (Co/C, 0.5Ru/C, and

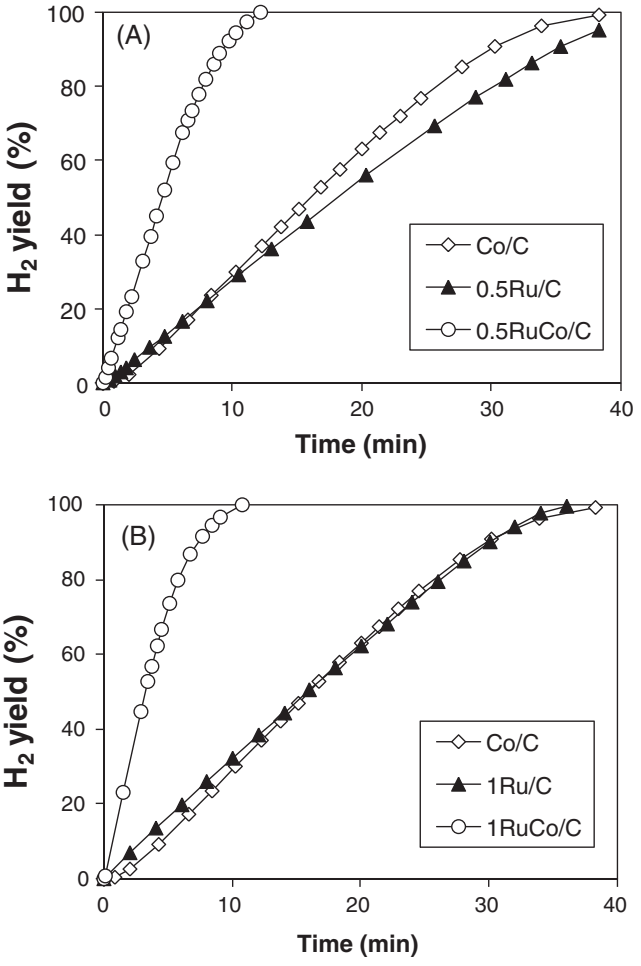


**FIGURE 1** $H_2$ yields in $NaBH_4$ hydrolysis ($T$ = 35°C) as a function of reaction time over carbon supported; A, 0.5Ru-Co and B, 1Ru-Co series (samples reduced in situ in flowing $H_2$ at 300°C for 1 h)

0.5RuCo/C samples) whereas in Figure 1B, the series with higher (1 wt%) Ru content (Co/C, 1Ru/C, and 1RuCo/C samples) is reported. The following trend of activity was observed: 1RuCo/C > 0.5RuCo/C > > 1Ru/C ≈ Co/C > 0.5Ru/C. It must be underlined that the activity of Ru-Co bimetallic catalysts sensibly exceeded the sum of the activities of corresponding monometallic samples, as also confirmed by the kinetic constants reported in Table 1. The good linearity of $H_2$ yield versus reaction time observed in the first portion of the data indicates that the reaction of $NaBH_4$ hydrolysis over mono and bimetallic Ru-Co/carbon catalysts, under the experimental conditions used, is zero order with regard to the hydride concentration. This accords with literature on other Ru/carbon samples under similar temperature and $NaBH_4$ concentration conditions.[19,41] Considering a zero reaction order, kinetic constants and activation energies were computed for all investigated catalysts and reported in Table 1. It is possible to note that activation energies (Ea) exhibit comparable values (56-69 kJ·mol$^{-1}$) with those described in the literature on variously supported ruthenium catalysts.[11,12,19,20,41] Noteworthy, Ea values reported in the literature appear strongly dependent on the support, the Ru content, and the metal precursor used.

The hydrolysis of ammonia borane (Figure 2) exhibited quite a different behavior than that of sodium borohydride. In fact, in the AB hydrolysis, the bimetallic 0.5RuCo/C sample had slightly better performance compared to the monometallic 0.5Ru/C one (Figure 2A), whereas no increase in the activity was found on the bimetallic sample with higher amount of Ru (1RuCo/C sample, Figure 2B). The order of activity was 0.5RuCo/C > 1Ru/C ≈ 1RuCo/C > 0.5Ru/C > > Co/C. Assuming also in this case a zero-order reaction, the rate constants for $H_2$ production were calculated at different temperatures from the slope of the linear part of each plot given in Figure 2 and used to estimate the Ea with Arrhenius equation. The apparent Ea for the hydrolysis of AB (Table 2) over Ru catalysts were similar to those reported in the literature for other supported ruthenium catalysts.[27,37,42] Interestingly, the Co/C sample exhibited an activation energy (57 kJ·mol$^{-1}$) much higher than monometallic Ru/C and bimetallic Ru-Co/C samples, which showed Ea ranging between 29 and 35 kJ/mol. Similar activation energy was reported for the AB hydrolysis using Co/γ-$Al_2O_3$.[43]

It is important to underline that both for SB and AB hydrolysis the activity was almost unchanged reusing the same lot of catalyst, after filtration and water washing, for 3 consecutive experiments, pointing to a good stability of the catalytic system.

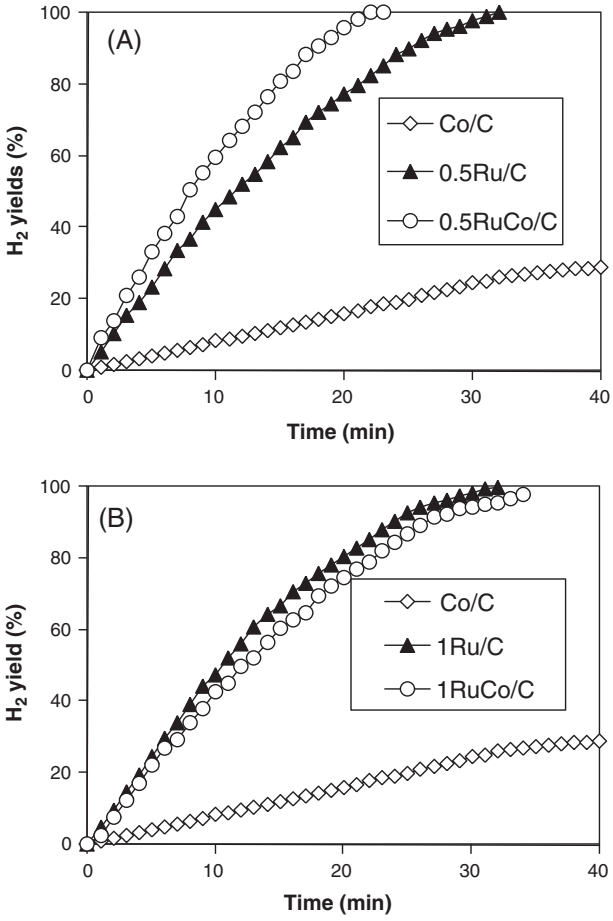


**FIGURE 2** $H_2$ yields in $NH_3BH_3$ hydrolysis ($T$ = 35°C) as a function of reaction time over carbon supported; A, 0.5Ru-Co and B, 1Ru-Co series (samples reduced in situ in flowing $H_2$ at 300°C for 1 h)

**TABLE 1** Kinetic data of SB hydrolysis of investigated samples

| k × 10$^{-2}$ ($L_{H2}$ $g_{cat}^{-1}$·min$^{-1}$) | | | | | |
|---|---|---|---|---|---|
| **Catalyst** | **15°C** | **25°C** | **35°C** | **45°C** | **Ea, kJ·mol$^{-1}$** |
| Co/C | - | 39 | 88 | 201 | 64.6 |
| 0.5Ru/C | - | 37 | 87 | 207 | 67.8 |
| 1Ru/C | - | 35 | 89 | 206 | 69.8 |
| 0.5RuCo/C | 67 | 159 | 340 | - | 59.7 |
| 1RuCo/C | 73 | 155 | 342 | - | 56.3 |

**TABLE 2** Kinetic data of AB hydrolysis of investigated samples

| k × 10$^{-2}$ ($L_{H2}$ $g_{cat}^{-1}$·min$^{-1}$) | | | | |
|---|---|---|---|---|
| **Catalyst** | **25°C** | **35°C** | **45°C** | **Ea, kJ·mol$^{-1}$** |
| Co/C | 3 | 5 | 13 | 57.0 |
| 0.5Ru/C | 11 | 20 | 27 | 35.5 |
| 1Ru/C | 18 | 25 | 39 | 30.1 |
| 0.5RuCo/C | 19 | 27 | 43 | 31.2 |
| 1RuCo/C | 16 | 24 | 33 | 29.3 |

## 3.2 | Catalyst characterization

Figure 3 shows the $H_2$-TPR profiles of investigated samples in terms of $H_2$ consumption versus temperature (from 50°C to 500°C). For all samples, it is possible to note two main hydrogen consumption intervals, the first one at lower temperature (between 200°C and 300°C) and the second at higher temperature (between 300°C and 450°C). To get a better insight in the reduction features of investigated samples, deconvolution of the TPR peaks was performed and the results are depicted in Figure 4 (monometallic samples) and Figure 5 (bimetallic samples). The estimation of the $H_2$ consumption related to the deconvoluted peaks is summarized in Table 3. In the low temperature zone, the monometallic Co sample (Co/C, Figure 4A) shows a broader signal in the 200°C to 320°C region, deconvoluted in two peaks at 242°C and 296°C, respectively. According to the literature,[44-46] the lower temperature peak can be assigned to the $H_2$-assisted decomposition of the cobalt nitrate precursor according to the reaction: $3Co(NO_3)_2 + 8H_2 \rightarrow Co_3O_4 + 6NO + 8H_2O$.[47,48] The formation of NO is confirmed by the analysis of the gases produced during TPR with online quadruple mass spectrometer, as shown by the peak of the m/z 30 mass signal in the same temperature range (inset of Figure 4A). The reduction feature at 296°C can be ascribed to the subsequent reduction of $Co_3O_4$ to CoO. Data reported in Table 3 indicate that the $H_2$ consumptions of both reduction features are around 3 times lower than those expected for the stoichiometric reactions above reported.

In the low temperature zone, the monometallic Ru samples (0.5Ru/C and 1Ru/C, Figures 4B,C) exhibit a single reduction peak with a maximum at 218°C. In this latter case, however, no formation of NO is visible (inset Figures 4B,C), reasonably considering that the reduction of the Ru nitrosylnitrate precursor, $Ru(NO)(NO_3)_3$, proceeds directly to nitrogen according to the following reaction: $Ru(NO)(NO_3)_3 + 10H_2 \rightarrow Ru + 2\ N_2 + 10H_2O$.

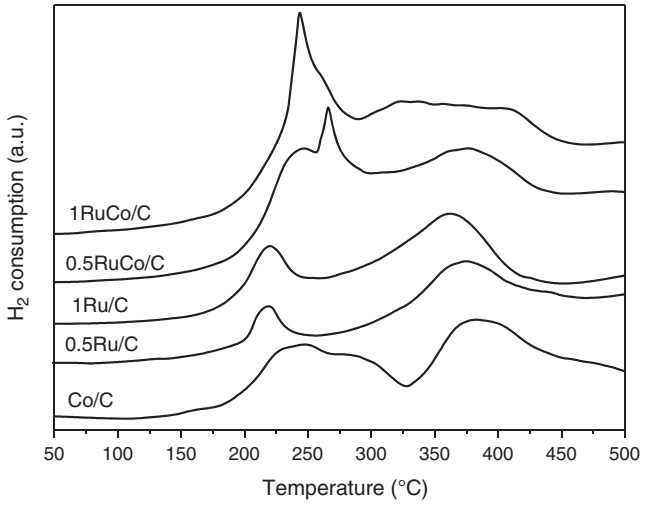


**FIGURE 3** $H_2$-TPR profiles of carbon supported Ru-Co catalysts (samples dried in air at 120°C for 2 h)

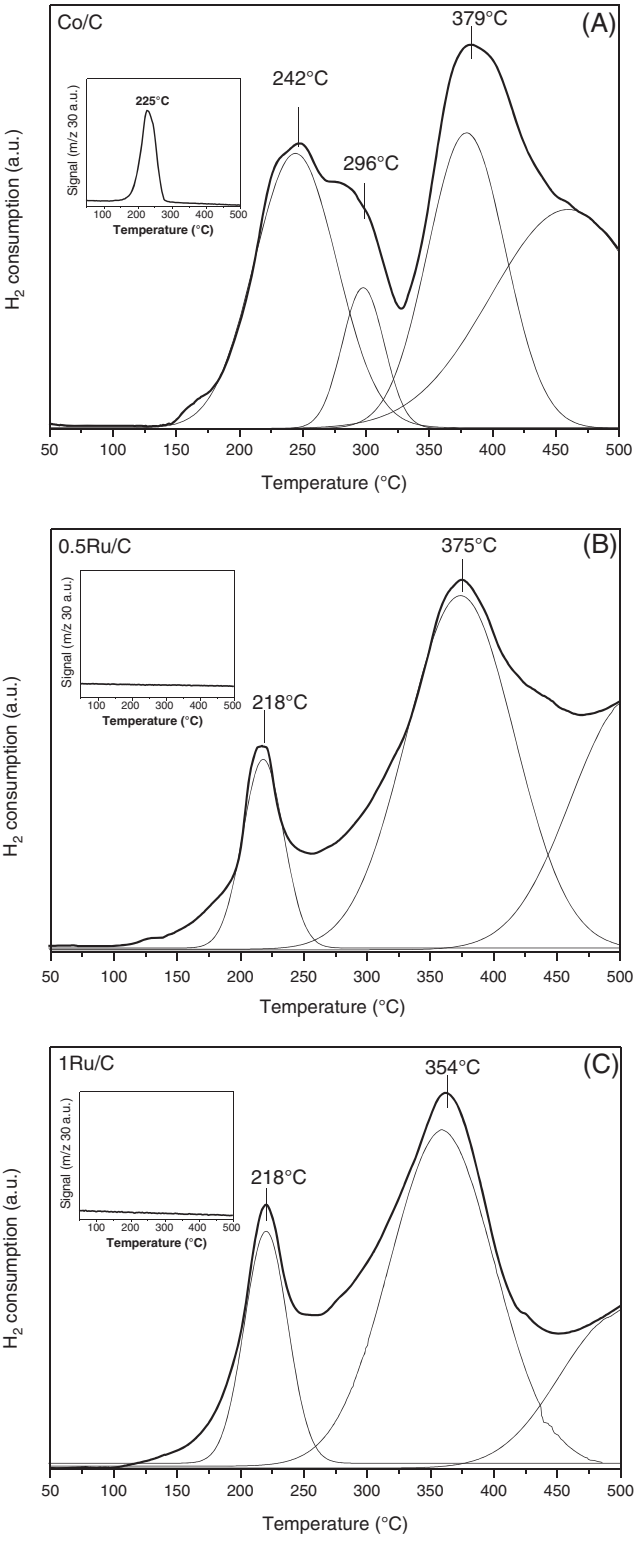


**FIGURE 4** $H_2$-TPR profiles with peaks deconvolution for A, Co/C; B, 0.5Ru/C; and C, 1Ru/C. On the inset, the NO formation as a function of the temperature

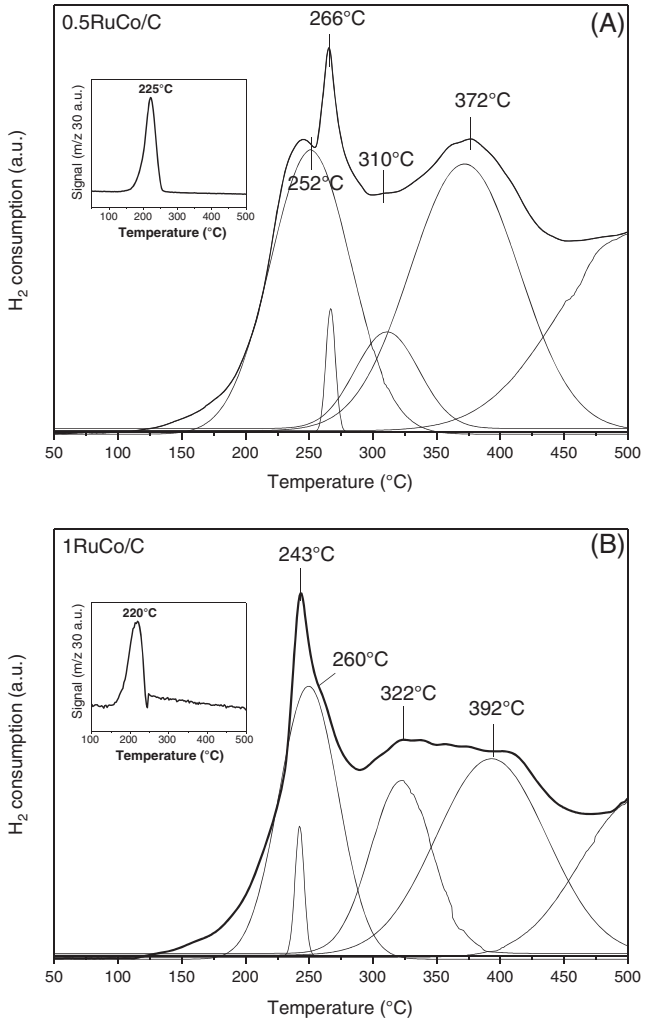


**FIGURE 5** $H_2$-TPR profiles with peaks deconvolution for A, 0.5RuCo/C and B, 1RuCo/C. On the inset, the NO formation as a function of the temperature

This is in good agreement with $H_2$ consumption data of Table 3. Unfortunately, due to the high background noise of the $N_2$ mass signals (m/z 28 and 14), the formation of molecular nitrogen was not observed.

Figure 5 illustrates the reduction pattern of the bimetallic samples. In particular, the deconvolution of the reduction peak of the 0.5RuCo/C sample reveals two features at 252°C and 266°C reasonably assigned to the contemporaneous reduction of cobalt nitrate and ruthenium species, as confirmed by the formation of NO (see the inset in Figure 5A). The formation of NO was detected also for the 1RuCo/C sample (Figure 5B) that exhibits a large peak at 243°C with a component at 260°C, also in this case, ascribed to the contemporaneous reduction of cobalt and ruthenium precursors. The components at 310°C (0.5RuCo/C) and 322°C (1RuCo/C) were reasonably assigned to the reduction of $Co_3O_4$ to CoO. Noticeably on the bimetallic samples, the reduction peaks attributed to ruthenium and cobalt species are shifted to higher temperature compared to the monometallic catalysts, pointing to a harder reduction of the metal precursors[49,50] and a stronger metal-support interaction occurring when Ru-Co bimetallic nanoparticles are present on the carbon support. Interestingly, the $H_2$ consumption of the bimetallic samples for the above reduction features exceeds the sum of those of the corresponding monometallics (Table 3). Even though it is not possible to discriminate between the single reduction components, this behavior suggests that on bimetallic Ru-Co samples a higher amount of $Co^{2+}$ was formed during the reduction process.

In the high temperature zone, all samples show a main $H_2$ consumption broad peak in the 350°C to 400°C range. According to the mass signals (Figure 6), this feature can be ascribed to the methanation of reactive carbon species of the support. In fact, on each sample, the m/z 15 signal gradually increased and reached a maximum in the same temperature range at which the high temperature $H_2$ consumption took place. Interestingly, the presence of ruthenium seems to favor the methanation process, with all Ru-based samples (0.5Ru/C, 1Ru/C, 0.5RuCo/C, and 1RuCo/C) showing peaks at lower temperature with higher $H_2$ consumption compared to the Co/C sample. The $H_2$ consumption occurring at $T > 400$°C, clearly visible in the deconvolved TPR profiles of all samples (Figures 4 and 5), can be reasonably ascribed to the

**TABLE 3** $H_2$-TPR quantification for investigated samples

| Catalyst | T peaks, °C | $H_2$ uptake, mmol/$g_{cat}$ | T peaks, °C | $H_2$ uptake, mmol/$g_{cat}$ | T peaks, °C | $H_2$ uptake, mmol/$g_{cat}$ |
|---|---|---|---|---|---|---|
| Co/C | 242 | 1.76 (4.5)[a] | 296 | 0.46 (1.1)[c] | 379 | 1.78 |
| 0.5Ru/C | 218 | 0.50 (0.49)[b] | - | - | 375 | 3.21 |
| 1Ru/C | 218 | 0.90 (0.98)[b] | - | - | 354 | 3.18 |
| 0.5RuCo/C | 252-266 | 3.31 | 310 | 0.57 | 372 | 3.96 |
| 1RuCo/C | 243-260 | 3.10 | 322 | 0.54 | 392 | 3.84 |

[a]In parentheses is the expected stoichiometric $H_2$ consumption for the $H_2$-assisted decomposition of the cobalt nitrate.

[b]In parentheses is the expected stoichiometric $H_2$ consumption for the reduction of Ru nitrosylnitrate.

[c]In parentheses is the expected stoichiometric $H_2$ consumption for the $Co_3O_4$ to CoO reduction.

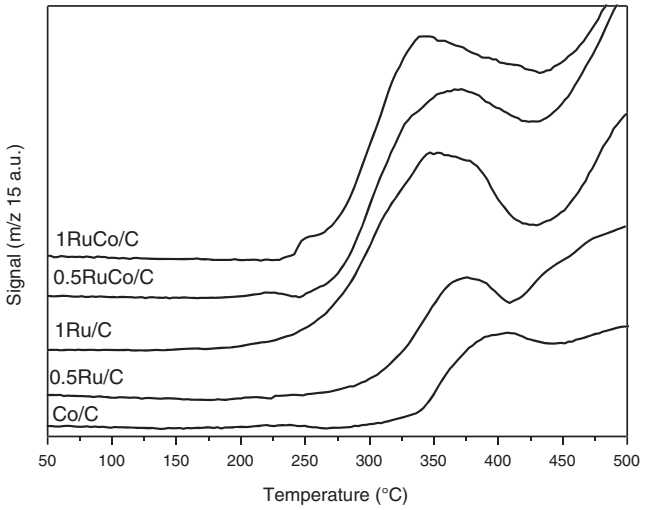


**FIGURE 6** Methane formation as a function of the temperature for tested catalysts

gasification of less reactive carbon bulk species, as confirmed by the corresponding significant increase in the m/z 15 mass signal due to methane formation[51] (Figure 6). According to the literature, the reduction of CoO to metallic cobalt occurs at $T > 350°C$,[52,53] overlapping with the methanation of reactive carbon species of the support, which takes place in the same temperature range, thus making impossible an affordable quantification of $Co^{2+} \rightarrow Co°$ reduction degree.

Table 4 summarizes the results of XPS analysis. These data pointed out an increase in the amount of surface Co species in the RuCo/C samples with respect to the monometallic Co sample, whereas the quantity of surface Ru species remains almost the same as in the monometallic Ru samples. Concerning ruthenium analysis, both spectra, Ru $3d_{5/2}$ and Ru $3p_{3/2}$ were collected. Due to the overlap of Ru $3d_{3/2}$ region with C 1s, a careful fitting procedure was needed to discriminate the binding energy position of the Ru $3d_{5/2}$ spin-orbit component, listed in the table along with the Ru $3p_{3/2}$ binding energy. The Ru $3d_{5/2}$ binding energy value in the single metal samples is at 281.2 ± 0.1 eV typical of $Ru^{4+}$ species such as in $RuO_2$ oxide.[54-56] The significant high energy shift observed in the bimetallic Ru-Co samples (281.8 ± 0.2 eV) is an indication of charge depletion on the Ru ions.[55,56] It was possible to fit the Ru $3p_{3/2}$ spectra with two components, a most intense one at a lower binding energy due to the $Ru^{4+}$ and a weaker component at high energy attributable to a more oxidized ruthenium.

The Co 2p spectra agreed with the presence of the mixed oxide $Co_3O_4$ formed by CoO and $Co_2O_3$. Indeed, the low energy peak at 779.7 ± 0.1 eV is typical of $Co^{3+}$ whereas the signal at 781.6 ± 0.1 eV with a large shake up satellite is typical of $Co^{2+}$.[55]

Given the overlapping of the Ru 3d and the C 1s energies, for quantification purpose, the Ru $3p_{5/2}$ peak was used. As reported in Table 4 and as expected from the adopted impregnation procedure, the larger values of experimental XPS derived Co/C and Ru/C atomic ratios as compared to the corresponding analytical ratios indicated metal surface segregation. The slight decrease of the Co/C, observed in the bimetallic samples was likely due to ruthenium segregating over the cobalt oxide species.

Figure 7 displays the XRD patterns of the investigated catalysts. The carbon support was present as amorphous phase characterized by the two broad signals[57] at $2\theta = 25.6°$ and 43.7°. The patterns of the monometallic

**TABLE 4** X-ray photoelectron spectroscopy binding energies (eV) and atomic ratios of investigated samples

| Catalyst | Co $2p_{3/2}$ (FWHM)[a] | Ru $3d_{5/2}$ (FWHM) | Ru $3p_{3/2}$ (FWHM) | O 1s (%) | Co/C[b] | Ru/C[a] |
|---|---|---|---|---|---|---|
| Co/C | 779.9 (2.3) | | | 531.3 (49) | 0.13 (0.02) | |
| | | | | 529.9 (40) | | |
| | 781.6 (2.3) | | | 532.7 (11) | | |
| 0.5Ru/C | | 281.3 (2.0) | 463.1 (4.2) | 531.0 (40) | | 0.01 (0.0006) |
| | | | 466.4 (4.2) | 533.3 (33) | | |
| | | | | 535.7 (27) | | |
| 1Ru/C | | 281.2 (1.7) | 463.0 (4.0) | 530.7 (59) | | 0.02 (0.001) |
| | | | | 532.8 (32) | | |
| | | | 466.0 (4.0) | 534.9 (0.9) | | |
| 0.5RuCo/C | 779.9 (2.4) | 282.0 (2.7) | 462.9 (5.5) | 529.8 (47) | 0.05 (0.02) | 0.01 (0.0007) |
| | | | | 531.4 (41) | | |
| | 781.7 (2.4) | | | 533.3 (12) | | |
| 1RuCo/C | 779.7 (2.3) | 281.6 (2.4) | 462.8 (4.9) | 529.8 (52) | 0.10 (0.02) | 0.03 (0.001) |
| | 781.5 (2.3) | | | 531.3 (38) | | |
| | | | | 533.2 (10) | | |

[a]Full width at half maximum.

[b]The values in parentheses refer to the analytical atomic ratios.

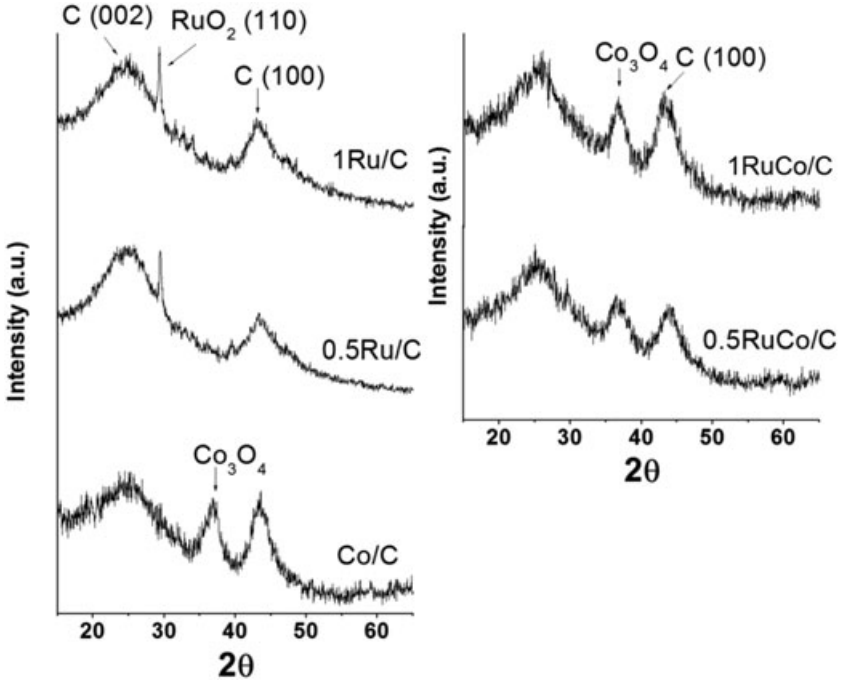


**FIGURE 7** X-ray diffraction patterns of tested catalysts (samples reduced ex situ in flowing $H_2$ at 300°C for 1 h)

ruthenium catalysts exhibited a peak at 2θ = 29.4°, attributed to $RuO_2$ (110) reflection of a tetragonal rutile structure. The absence of the other peaks typical for this structure reflects a strong preferential crystallographic orientation. The peak at 2θ = 29.4° is hardly present in the patterns of the RuCo bimetallic samples containing clearly the peak at 2θ = 36.8° typical of $Co_3O_4$.[58] According to these results, amorphous or $RuO_2$ particle sizes smaller than 4 nm, limit of detection under the stated experimental conditions, are suggested. On the contrary, larger $RuO_2$ particles in the 5- to 6-nm size range are present in the case of monometallic 1Ru/C and 0.5Ru/C samples. This observation points out a superior dispersion of ruthenium particles on the carbon support when Co is also present. The average crystallite sizes of the particles, computed by the Scherrer equation on the diffraction peaks of Co (2θ = 36.8°) for Co/C, 1RuCo/C and 0.5RuCo/C and of $RuO_2$ (1 1 0, 2θ = 29.4°) for 1Ru/C and 0.5Ru/C, are reported in Table 5. A decrease of the crystallite size of cobalt oxide species in the bimetallic samples (around 8 nm) as compared to the monometallic Co/C sample (around 12 nm) can be observed.

The supported metal catalysts dispersion, ie, the fraction of the surface to the whole number of metal species, is correlated to the metal particles size. The volume of CO chemisorbed and the corresponding metallic dispersion values of investigated samples are reported in Table 5. It must be underlined that in the case of the Ru-Co bimetallic samples, the estimation of the volume of CO chemisorbed on each single species is a tricky question in so as both species (Ru or Co oxide) are able to chemisorb CO. Anyway, we took into account that (*a*) ruthenium is present in small amount (0.5-1% wt) compared to Co (10% wt), (*b*) Ru monometallic samples exhibited quite high dispersion values (80% and 76%, respectively, for 0.5Ru/C and 1Ru/C), and (*c*) XRD data pointed out a homogeneous Ru distribution on the surface of the bimetallic Ru-Co catalysts and smaller Ru particles than the monometallic Ru. Therefore, we consider it reasonable to estimate the amount of CO chemisorbed on cobalt oxide species by subtracting the volume of CO consumed by Ru-Co samples and the theoretical volume of CO chemisorbed by the corresponding monometallic Ru catalyst assuming a 100% Ru dispersion. The obtained data, reported in Table 5, show that the Ru-Co bimetallic samples exhibit higher cobalt oxide species dispersion values (3.8% and 6.2%, respectively, for 0.5RuCo/C and 1RuCo/C) than the monometallic cobalt catalyst (0.87%),

**TABLE 5** Volume of CO chemisorbed, active species dispersion and crystallite size of investigated samples

| Catalyst | CO Chemisorbed, $mL_{STP}$ | Dispersion, %[b] | Crystallite Size, nm[c] |
|---|---|---|---|
| Co/C | 0.98 | 0.87 | 12.5 ($Co_3O_4$) |
| 0.5Ru/C | 2.6 | 80 | 5.2 ($RuO_2$) |
| 1Ru/C | 4.9 | 76 | 5.8 ($RuO_2$) |
| 0.5RuCo/C | 4.44 (1.84[a]) | 3.8 ($Co_3O_4$) | 8.8 ($Co_3O_4$) |
| 1RuCo/C | 7.33 (2.43 [a]) | 6.2 ($Co_3O_4$) | 8.2 ($Co_3O_4$) |

[a]The estimated volume of CO chemisorbed on cobalt oxide species.

[b]Estimated by CO chemisorption.

[c]Calculated by Scherrer equation.

evidencing a decrease of the cobalt oxide particle size in presence of ruthenium, as confirmed by XRD data.

The TEM microphotographs of the investigated samples are reported in Figure 8. The low Ru loading and the low contrast between Ru and the carbon support did not allow an affordable determination of the Ru particle size both in Ru and Ru-Co catalysts whereas it was possible to estimate the size of Co oxide nanoparticles, which were 10 to 12 nm (Figure 8C) in the monometallic Co/C sample and 5 to 8 nm in the bimetallic 0.5RuCo/C sample (Figure 8D). The TEM data confirm the XRD and CO chemisorption results before discussed.

## 4 | DISCUSSION

The results above described pointed out that the presence of cobalt oxide species in the Ru/activated carbon system affects in different ways the catalytic activity of the hydrolysis of $NaBH_4$ and $NH_3BH_3$. In particular, in the $NaBH_4$ hydrolysis, the bimetallic samples, 1RuCo/C and 0.5RuCo/C, showed an activity higher than the sum of those of monometallics samples (Figure 1). As reported in the literature,[11,19,59] active sites in $NaBH_4$ hydrolysis consist of adjacent metal atoms on which both reagents ($H_2O$ and $NaBH_4$) adsorb, giving an activated complex, according to the Langmuir-Hinshelwood model. This is also consistent with the zero reaction order found with respect to $NaBH_4$. The characterization results hinted at the occurrence of a reciprocal interaction between ruthenium and cobalt oxide giving rise to some effects: (*a*) Ru surface enrichment in the bimetallic samples as pointed out by XPS; (*b*) decrease in the size of both Ru and $CoO_x$ nanoparticles as pointed out by XRD (both for Ru and Co) and TEM (only for Co); (*c*) enhanced reducibility of the $Co_3O_4$ to CoO according to TPR. The synergetic interaction between ruthenium and the cobalt oxide species is mostly due to electronic effects, which become important when the electronegativity of metals is significantly different (in this case, 2.3 for Ru and 1.88 for Co), and to a stabilization role of the cobalt oxide species towards the Ru metallic phase[60] or of the Ru towards the CoO phase. As

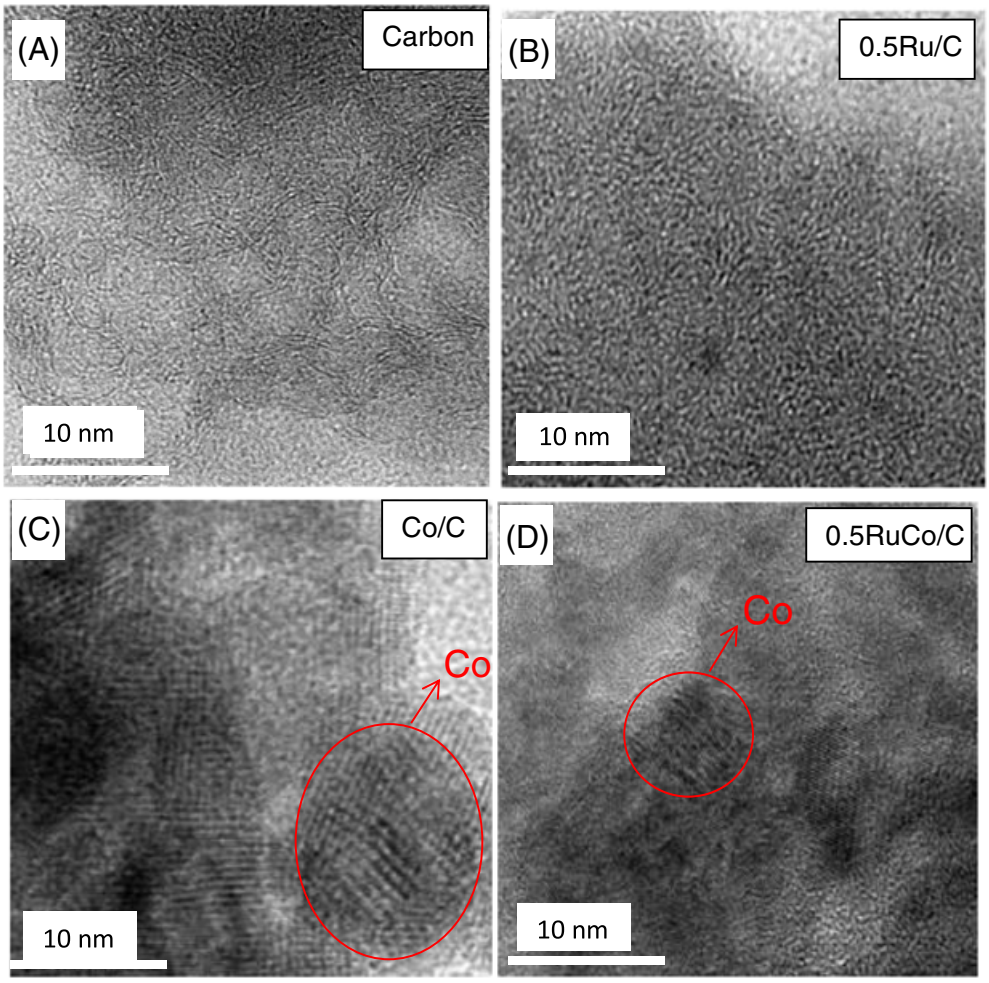


**FIGURE 8** Transmission electron microscopy photos of investigated samples: A, carbon support; B, 0.5Ru/C; C, Co/C; and D, 0.5RuCo/C (samples reduced ex situ in flowing $H_2$ at 300°C for 1 h) [Colour figure can be viewed at wileyonlinelibrary.com]

reported in the XPS data (Table 4), the high energy shift of the Ru 3d binding energy is indicative of an electron interaction of Ru with Co leading to an electron depletion over the ruthenium element. Moreover, the mutual reduction of particle sizes is not new in mixed oxide morphology and it is attributable to the insertion of either ion into the other oxide lattice.[61]

On account of the reported characterization results, it can be proposed that metallic $Ru^{\circ}$ species are formed during the pretreatment of the catalysts before the activity tests (reduction with $H_2$ at 300°C), promoting the activation of hydrogen and then enhancing the reduction degree of the cobalt precursor salt to $Co^{2+}$ (as confirmed by TPR) and therefore the number of cobalt oxide species nucleation centers. It is also highly probable that a subsequent reduction of cobalt and ruthenium species takes place in the hydride reaction medium. Therefore, the state of the catalyst before the catalytic experiment has a key role in determining the state of the active phase formed in situ. Moreover, as pointed out by XRD, XPS, and TEM characterizations, the interaction between ruthenium and cobalt oxide favors the formation of smaller Ru and Co particles with a better dispersion on the carbon support. The presence of smaller active metal particles is certainly beneficial for the catalytic activity of bimetallic Ru-Co catalysts towards the $NaBH_4$ hydrolysis, which has been reported to be a structure sensitive reaction, activity of catalysts depending on the metal particles size. In particular, the activity was found to increase on decreasing the particle size of metal active sites,[19,62,63] at least down to a diameter of around 2 nm, which was accounted to be the optimal one for the $NaBH_4$ hydrolysis both over Ru[19] and Pt catalysts.[62] Unfortunately, even though XRD data (Figure 7) point out that in the bimetallic samples, both Ru and Co particles are smaller than those of the corresponding monometallic catalysts; the low contrast between Ru and the carbon support in TEM images does not allow to determine the real Ru particle size, then making impossible to establish with certainty the role of the Ru particle size.

Interestingly, the positive effect of the Ru-Co interaction in the bimetallic Ru-Co samples was sensibly less evident in the case of the $NH_3BH_3$ hydrolysis. For this reaction, in fact, the bimetallic catalysts exhibited a catalytic behavior only slightly better or similar to that of the corresponding Ru monometallic sample. To explain the different behaviors of bimetallic Ru-Co/C samples towards AB and SB hydrolysis, we must take into account that the activity of the monometallic Co catalyst towards AB hydrolysis is much lower than that found in the SB hydrolysis, Co/C sample being poorly active, more than one order of magnitude lower than Ru/C samples (Figure 2 and Table 2), whereas a comparable activity was observed in the SB hydrolysis over Ru and Co monometallic catalysts (Figure 1 and Table 1). The lower activity of monometallic Co catalysts compared to Ru ones for the AB hydrolysis was in accordance with results previously reported in the literature.[44,55,64] Therefore, in the case of the AB hydrolysis, the better dispersion of the cobalt oxide species active sites achieved in the Ru-Co/C bimetallic samples with respect to the monometallic Co/C does not provide any significant improvement in the catalytic activity, pointing out that Ru sites are much more important than Co ones in addressing the AB hydrolysis activity of bimetallic Ru-Co/C catalysts. This is in accordance with the fact that catalytic activity of 1RuCo/C towards AB hydrolysis was slightly lower compared to 0.5RuCo/C (Figure 2), notwithstanding the cobalt oxide species dispersion of 1RuCo/C was approximately two times higher of 0.5RuCo/C (Table 5). Such results well agree with kinetic data reported in Table 2 for AB hydrolysis, indicating much lower values of Ea of monometallic Ru samples (30-35 kJ/mol) as compared to monometallic Co (57 kJ/mol). It must be finally underlined that the 1RuCo/C catalyst exhibits the lowest value of $E_a$ (29 kJ/mol) compared to other RuCo systems reported in the literature (see Table 6). This value was only slightly higher than that observed on a highly active Ni-Mo/graphene catalyst (21.8 kJ/mol).[65]

It can be then supposed that the different relative reactivity of Co and Ru towards the SB and AB hydrolysis can account for the different behavior of the bimetallic Ru-Co/C catalysts in the above reactions. In fact, also for AB hydrolysis, a Langmuir-Hinshelwood reaction model has been proposed,[66,67] involving the interaction between the $NH_3BH_3$ molecule and the metal particle on the surface forming an activated complex species (rate-determining step), with subsequent release of $H_2$ after water interacts with the metal-H species.[37,67] The stronger affinity between ammonia released during the hydrolysis and the cobalt oxide species may negatively affect the catalytic reaction by inhibiting the desorption

**TABLE 6** Comparison of AB hydrolysis activation energies over RuCo/C catalysts (this work and other RuCo catalysts reported in the literature)

| Catalyst | Support | $E_a$, kJ/mol | Reference |
|---|---|---|---|
| RuCo/C | Activated carbon | 29.3 | This work |
| RuCo/γ-$Al_2O_3$ | Alumina | 50 | Rachiero et al[37] |
| RuCo@MIL-96 | Nanofibrous metal-organic framework MIL-96(Al) | 36.0 | Lu et al[64] |
| RuCo/$Ti_3C_2X_2$ | Titanium carbide | 31.1 | Li et al[55] |

of the reaction products.[37,68] As a result, the ruthenium containing samples are the most active for the $NH_3BH_3$ reaction.

## 5 | CONCLUSIONS

Data described in this work allow to state that the addition of small amount of Ru boosts the catalytic performance of activated carbon supported Co catalysts towards the $NaBH_4$ hydrolysis. The activity of the bimetallic Ru-Co/carbon samples exceeds indeed the sum of the activities of monometallic catalysts. The characterization data pointed out a mutual interaction between ruthenium and cobalt oxide causing a decrease in the size of Ru and Co oxide nanoparticles. It was proposed that $Ru^{\circ}$, formed first during the reduction step of the Ru-Co samples, favors the $H_2$ activation, enhancing the reduction degree of the cobalt salt to $Co^{2+}$ and the number of cobalt oxide species nucleation centers. Reasonably, a subsequent reduction of cobalt and ruthenium species also occurs in the hydride reaction medium and therefore, we can conclude that the state of the catalyst before the catalytic experiment can determine the state of the active phase formed in situ. The enhancement of catalytic activity of the Ru-Co system was much less evident in the case of the $NH_3BH_3$ hydrolysis reaction and this was attributed to the much lower reactivity of Co species compared to Ru ones towards the hydrolysis of $NH_3BH_3$.

## ACKNOWLEDGEMENTS

We thank Dr Corrado Bongiorno (CNR-IMM Catania) for TEM measurements.

## ORCID

*R. Fiorenza* http://orcid.org/0000-0002-2773-0017
*S. Scirè* http://orcid.org/0000-0002-3060-0918
*A.M. Venezia* http://orcid.org/0000-0001-7197-875X

## REFERENCES

1. Moussa G, Romain M, Demirci UB, Şener T, Miele P. Boron-based hydrides for chemical hydrogen storage. *Int J Energy Res*. 2013;37:825-884.
2. Boran A, Erkan S, Ozkar S, Eroglu I. Kinetics of hydrogen generation from hydrolysis of sodium borohydride on Pt/C catalyst in a flow reactor. *Int J Energy Res*. 2013;37:443-448.
3. Ferey G. Hybrid porous solids: past, present, future. *Chem Soc Rev*. 2008;37:191-214.
4. Li G, Kobayashi H, Taylor J, et al. Hydrogen storage in Pd nanocrystals covered with a metal–organic framework. *Nat Mater*. 2014;13:802-806.
5. Junge H, Loges B, Beller M. Novel improved ruthenium catalysts for the generation of hydrogen from alcohols. *Chem Commun*. 2007;522-524.
6. Johnson TC, Morris DJ, Wills M. Hydrogen generation from formic acid and alcohols using homogeneous catalysts. *Chem Soc Rev*. 2010;39:81-88.
7. Solymosi F, Koós Á, Liliom N, Ugrai I. Production of CO-free $H_2$ from formic acid. A comparative study of the catalytic behavior of Pt metals on a carbon support. *J Catal*. 2011;279:213-219.
8. Huang ZM, Su A, Liu YC. Catalytic hydrolysis of sodium borohydride on Co catalysts. *Int J Energy Res*. 2013;37:1187-1195.
9. Demirci UB. The hydrogen cycle with the hydrolysis of sodium borohydride: a statistical approach for highlighting the scientific/technical issues to prioritize in the field. *Int J Hydrogen Energy*. 2015;40:2673-2691.
10. Kim JH, Lee H, Han SC, Kim HS, Song MS, Lee JY. Production of hydrogen from sodium borohydride in alkaline solution: development of catalyst with high performance. *Int J Hydrogen Energy*. 2004;29:263-267.
11. Crisafulli C, Scirè S, Salanitri M, Zito R, Calamia S. Hydrogen production through $NaBH_4$ hydrolysis over supported Ru catalysts: an insight on the effect of the support and the ruthenium precursor. *Int J Hydrogen Energy*. 2011;36:3817-3826.
12. Peng S, Fan X, Zhang J, Wang F. A highly efficient heterogeneous catalyst of Ru/MMT: preparation, characterization, and evaluation of catalytic effect. *Appl Catal Environ*. 2013;140-141:115-124.
13. Chowdhury AD, Agnihotri N, De A. Hydrolysis of sodium borohydride using Ru–Co-PEDOT nanocomposites as catalyst. *Chem Eng J*. 2015;264:531-537.
14. Demirci UB, Miele P. Cobalt in $NaBH_4$ hydrolysis. *Phys Chem Chem Phys*. 2010;12:14651-14665.
15. Bai Y, Wu C, Wu F, Yi B. Carbon-supported platinum catalysts for on-site hydrogen generation from $NaBH_4$ solution. *Mater Lett*. 2006;60:2236-2239.
16. Xu D, Zhang H, Ye W. Hydrogen generation from hydrolysis of alkaline sodium borohydride solution using Pt/C catalyst. *Cat Com*. 2007;8:1767-1771.
17. Walter JC, Zurawski A, Montgomery D, Thornburg M, Revankar S. Sodium borohydride hydrolysis kinetics comparison for nickel, cobalt, and ruthenium boride catalysts. *J Power Sources*. 2008;179:335-339.
18. Patel N, Patton B, Zanchetta C, et al. Pd-C powder and thin film catalysts for hydrogen production by hydrolysis of sodium borohydride. *Int J Hydrogen Energy*. 2008;33:287-292.
19. Crisafulli C, Scirè S, Zito R, Bongiorno C. Role of the support and the Ru precursor on the performance of Ru/Carbon catalysts towards $H_2$ production through $NaBH_4$ hydrolysis. *Catal Lett*. 2012;142:882-888.
20. Li Z, Li H, Wang L, et al. Hydrogen generation from catalytic hydrolysis of sodium borohydride solution using supported amorphous alloy catalysts (Ni–Co–P/$\gamma$-$Al_2O_3$). *Int J Hydrogen Energy*. 2014;39:14935-14941.

21. Wee JH, Lee KY, Kim SH. Sodium borohydride as the hydrogen supplier for proton exchange membrane fuel cell systems. *Fuel Process Technol*. 2006;87:811-819.
22. Demirci UB, Miele P. Sodium borohydride versus ammonia borane, in hydrogen storage and direct fuel cell applications. *Energ Environ Sci*. 2009;2:627-637.
23. Rusman NAA, Dahari M. A review on the current progress of metal hydrides material for solid-state hydrogen storage applications. *Int J Hydrogen Energy*. 2016;41:12108-12126.
24. Rakap M, Ozkar S. Zeolite confined palladium(0) nanoclusters as effective and reusable catalyst for hydrogen generation from the hydrolysis of ammonia-borane. *Int J Hydrogen Energy*. 2010;35:1305-1312.
25. Sullivan JA, Herron R, Phillips AD. Towards an understanding of the beneficial effect of mesoporous materials on the dehydrogenation characteristics of $NH_3BH_3$. *Appl Catal Environ*. 2017;201:182-188.
26. Song-Il O, Yan JM, Wang HL, Wang ZL, Jiang Q. High catalytic kinetic performance of amorphous CoPt NPs induced on CeOx for $H_2$ generation from hydrous hydrazine. *Int J Hydrogen Energy*. 2014;39:3755-3761.
27. Akbayrak S, Tanyıldızı S, Morkan I, Ozkar S. Ruthenium(0) nanoparticles supported on nanotitania as highly active and reusable catalyst in hydrogen generation from the hydrolysis of ammonia borane. *Int J Hydrogen Energy*. 2014;39:9628-9637.
28. Zahmakiran M, Özkar S. Zeolite framework stabilized rhodium(0) nanoclusters catalyst for the hydrolysis of ammonia-borane in air: Outstanding catalytic activity, reusability and lifetime. *Appl Catal Environ*. 2009;89:104-110.
29. Metin O, Özkar S. Hydrogen generation from the hydrolysis of ammonia-borane and sodium borohydride using water-soluble polymer-stabilized cobalt(0) nanoclusters catalyst. *Energy Fuel*. 2009;23:3517-3526.
30. Yan JM, Zhang XB, Han S, Shioyama H, Xu Q. Iron-nanoparticle-catalyzed hydrolytic dehydrogenation of ammonia borane for chemical hydrogen storage. *Angew Chem Int Ed*. 2008;47:2287-2289.
31. Jiang HL, Xu Q. Catalytic hydrolysis of ammonia borane for chemical hydrogen storage. *Catal Today*. 2011;170:56-63.
32. Demirci UB, Miele P. Cobalt-based catalysts for the hydrolysis of $NaBH_4$ and $NH_3BH_3$. *Phys Chem Chem Phys*. 2014;16:6872-6885.
33. Fiorenza R, Crisafulli C, Scirè S. $H_2$ purification through preferential oxidation of CO over ceria supported bimetallic Au-based catalysts. *Int J Hydrogen Energy*. 2016;41:19390-19398.
34. Crisafulli C, Scirè S, Maggiore R, Minicò S, Galvagno S. $CO_2$ reforming of methane over Ni–Ru and Ni–Pd bimetallic catalysts. *Catal Lett*. 1999;59:21-26.
35. Krishnan P, Yang TH, Lee WY, Soo KC. PtRu-$LiCoO_2$-an efficient catalyst for hydrogen generation from sodium borohydride solutions. *J Power Sources*. 2005;143:17-23.
36. Liu BH, Li ZP, Suda S. Nickel- and cobalt-based catalysts for hydrogen generation by hydrolysis of borohydride. *J Alloys Compd*. 2006;415:288-293.
37. Rachiero GP, Demirci UB, Miele P. Bimetallic RuCo and RuCu catalysts supported on $\gamma$-$Al_2O_3$. A comparative study of their activity in hydrolysis of ammonia-borane. *Int J Hydrogen Energy*. 2011;36:7051-7065.
38. JCPDS Powder Diffraction File. Int. Centre for Diffraction Data, Swarthmore; File No. 42-1467.
39. Shirley DA. High-resolution X-ray photoemission spectrum of the valence bands of gold. *Phys Rev B* **51972**. 4709-4714.
40. Sherwood PMA, Briggs D, Seah MP (Eds). *Practical Surface Analysis*. New York: Wiley; 1990:181.
41. Zhang J, Delgass WN, Fisher TS, Gore JP. Kinetics of Ru-catalyzed sodium borohydride hydrolysis. *J Power Sources*. 2007;164:772-781.
42. Basu S, Brockman A, Gagare P, et al. Chemical kinetics of Ru-catalyzed ammonia borane hydrolysis. *J Power Sources*. 2009;188:238-243.
43. Chandra M, Xu Q. Catalytic activities of non-noble metals for hydrogen generation from aqueous ammonia–borane at room temperature. *J Power Sources*. 2006;163:364-370.
44. Huang L, Xu Y. Studies on the interaction between ruthenium and cobalt in supported catalysts in favor of hydroformylation. *Catal Lett*. 2000;69:145-151.
45. Guczi L, Sundararajan R, Koppany Z, et al. Structure and characterization of supported ruthenium-cobalt bimetallic catalysts. *J Catal*. 1997;167:482-494.
46. Martínez A, Prieto G, Rollán J. Nanofibrous $\gamma$-$Al_2O_3$ as support for Co-based Fischer–Tropsch catalysts: pondering the relevance of diffusional and dispersion effects on catalytic performance. *J Catal*. 2009;263:292-305.
47. Wigzell FA, Jacson SD. The genesis of supported cobalt catalysts. *Appl Petrochem Res*. 2016;1-13.
48. Mehandjiev D, Nikolova-Zhecheva E. Mechanism of the decomposition of cobaltous compounds in vacuo. *Thermochim Acta*. 1980;37:145-154.
49. Crisafulli C, Maggiore R, Scirè S, Solarino L, Galvagno S. Effect of precursor on the catalytic behaviour of Ru-Cu/MgO. *J Mol Catal A Chem*. 1990;63:55-63.
50. Scirè S, Fiorenza R, Gulino A, Cristaldi A, Riccobene PM. Selective oxidation of CO in $H_2$-rich stream over ZSM5 zeolites supported Ru catalysts: an investigation on the role of the support and the Ru particle size. *Appl Catal Gen*. 2016;520:82-91.
51. Atamny F, Blöcker J, Dübotzky A, et al. Surface chemistry of carbon: activation of molecular oxygen. *Mol Phys*. 1992;76(4):851-886.
52. Li W, Yu SY, Meitzner GD, Iglesia E. Structure and properties of cobalt-exchanged H-ZSM5 catalysts for dehydrogenation and dehydrocyclization of alkanes. *J Phys Chem B*. 2001;105:1176-1184.
53. Qwabe LQ, Friedrich HB, Sooboo S. Preferential oxidation of CO in a hydrogen rich feed stream using Co-Fe mixed metal oxide catalysts prepared from hydrotalcite precursors. *J Mol Catal A Chem*. 2015;404-405:167-177.
54. Moulder JF, Stickle WF, Sobol PE, Bomben KD. *Handbook of X-ray Photoelectron Spectroscopy*. Eden Prairie, Minnesota: Perkin-Elmer Corporation; 1993.
55. Li X, Zeng C, Fan G. Magnetic RuCo nanoparticles supported on two-dimensional titanium carbide as highly active catalysts for

the hydrolysis of ammonia borane. *Int J Hydrogen Energy*. 2015;40:9217-9224.

56. Snytnikov PV, Sobyanin VA, Belyaev VD, Tsyrulnikov PG, Shitova NB, Shlyapin SA. Selective oxidation of carbon monoxide in excess hydrogen over Pt-, Ru- and Pd-supported catalysts. *Appl Catal Gen*. 2003;239:149-156.
57. Zhao J, Yang L, Li F, Yu R, Jin C. Structural evolution in the graphitization process of activated carbon by high-pressure sintering. *Carbon*. 2009;47:744-751.
58. Jansson J, Palmqvist AEC, Fridell E, et al. On the catalytic activity of $Co_3O_4$ in low-temperature CO oxidation. *J Catal*. 2002;211:387-397.
59. Liu BH, Li ZP. A review: hydrogen generation from borohydride hydrolysis reaction. *J Power Sources*. 2009;187:527-534.
60. Ragaini V, Pirola C, Vitali S, Bonura G, Cannilla C, Frusteri F. Stability of metallic ruthenium in Ru–Co supported silica catalysts. *Catal Lett*. 2012;142:1452-1460.
61. Shan W, Luo M, Ying P, Shen W, Li C. Reduction property and catalytic activity of $Ce_{1-X}Ni_XO_2$ mixed oxide catalysts for $CH_4$ oxidation. *Appl Catal Gen*. 2003;246:1-9.
62. Kojima Y, Suzuki K, Fukumoto K, et al. Hydrogen generation using sodium borohydride solution and metal catalyst coated on metal oxide. *Int J Hydrogen Energy*. 2002;27:1029-1034.
63. Park JH, Shakkthivel P, Kim HJ, et al. Investigation of metal alloy catalyst for hydrogen release from sodium borohydride for polymer electrolyte membrane fuel cell application. *Int J Hydrogen Energy*. 2008;33:1845-1852.
64. Lu D, Yu G, Li Y, et al. RuCo NPs supported on MIL-96(Al) as highly active catalysts for the hydrolysis of ammonia borane. *J Alloys Compd*. 2017;694:662-671.
65. Yao Q, Lu ZH, Huang W, Chen X, Zhu J. High Pt-like activity of the Ni–Mo/graphene catalyst for hydrogen evolution from hydrolysis of ammonia borane. *J Mater Chem A*. 2016;4:8579-8583.
66. Shang Y, Chen R, Jiang G. Kinetic study of $NaBH_4$ hydrolysis over carbon-supported ruthenium. *Int J Hydrogen Energy*. 2008;33:6719-6726.
67. Xu Q, Chandra M. Catalytic activities of non-noble metals for hydrogen generation from aqueous ammonia–borane at room temperature. *J Power Sources*. 2006;163:364-370.
68. Rachiero GP, Demirci UB, Miele P. Facile synthesis by polyol method of a ruthenium catalyst supported on γ-Al2O3 for hydrolytic dehydrogenation of ammonia borane. *Catal Today*. 2011;170:85-92.

**How to cite this article:** Fiorenza R, Scirè S, Venezia AM. Carbon supported bimetallic Ru-Co catalysts for $H_2$ production through $NaBH_4$ and $NH_3BH_3$ hydrolysis. *Int J Energy Res*. 2017;1–13. https://doi.org/10.1002/er.3918